A Fully Tetrahedral and Highly Corner-Sharing Network Model of $ZnCl_2$ Glass and its Comparison to SiO_2 Glass

Laura A. Swansbury and Gavin Mountjoy*

School of Physical Sciences, University of Kent, Canterbury, Kent, CT2 7NH, U.K.

Abstract:

Zinc chloride, $ZnCl_2$, is intermediate between a strong and a fragile glass former. During computational simulations, it is therefore important to account for ion polarizability. This, together with the lack of suitable interatomic potential parameters is the likely cause for the lack of modelling studies on $ZnCl_2$ glass which contain a high degree of $ZnCl_4$ tetrahedral units. Through using accurate interatomic potential parameters and applying the adiabatic core-shell model, the first fully tetrahedral model of $ZnCl_2$ glass was obtained. The Cl-Zn-Cl bond angle of 109° reproduced the ideal tetrahedral bond angle, and the calculated total neutron and x-ray structure factors closely replicated experimental findings. While 86% of the $ZnCl_4$ tetrahedral units were corner-sharing, 14% were found to be edge-sharing. This led to two distinct contributions in both the Zn-Cl-Zn bond angle distribution and in the Zn···Zn nearest neighbour peaks being seen. These are not apparent in studies based on neutron diffraction. By comparing the intermediate glass former $ZnCl_2$ to the strong glass former SiO_2, marked differences in ring statistics became apparent. The Zn-Cl-Zn bond angle of around 110° enabled 3-membered rings to form in significant proportions. In contrast, 3-membered rings were only present in SiO_2 glass as defects. By calculating the $ZnCl_2$ and SiO_2 partial structure factors, strong similarities became visible after scaling according to nearest neighbour distances. Although it was apparent that the main contributions to the FSDPs came from cation-anion correlations, the relative scaling of the FSDP positions in $ZnCl_2$ and SiO_2 glass was not understood.

Introduction:

Zinc chloride ($ZnCl_2$) is an intermediate glass forming system, in between that of a strong (e.g. SiO_2) and a fragile (e.g. $BeCl_2$ [1]) glass former [1]. The $ZnCl_2$ system is based on tetrahedral structural units ($ZnCl_4$) and is known to have a high tendency towards glass formation [2]. Another well-known intermediate glass former with tetrahedral units is germanium selenide ($GeSe_2$), although the presence of homopolar bonding due to its more covalent nature complicates the connectivity of the glass network [3]. It is therefore intuitive to consider the $ZnCl_2$ system in order to gain insight into the structural effects of polarizable anions in glasses. To study this on an atomic scale, computational simulation can be used. As will be described below, previous computational studies on $ZnCl_2$ glass have not been successful in presenting the completely tetrahedral network structure that is expected. This may be caused both by the complexity of accounting for ion polarizability, and the lack of available suitable interatomic potential parameters [2], [4].

One type of computational simulation is classical molecular dynamics simulation. This relies on using interatomic potential parameters, the simplest of which are of rigid-ion (RI) form. These treat the atoms as rigid spheres and fail to account for ion polarizability, but do permit large system sizes to be modelled over relatively long timescales. Kumta *et al.* [5] modelled a $ZnCl_2$ glass system using RI interatomic potentials, but the model only comprised of 324 atoms. The average Zn-Cl coordination number of 4.96 did not correspond to tetrahedral structural units. In fact, 40% of the structural units were reported to be $ZnCl_6$ structural units, casting doubt over the interatomic potential parameters used.

In contrast to classical molecular dynamics, first principles simulation considers the electronic configuration of atoms. However, a limited system size can only be modelled for a relatively short period. The liquid $ZnCl_2$ model obtained by Alsayoud et al. [6] using first principles simulation contained 108 atoms and was quenched from 2000K to 600K at a rate of 1.8×10^{14}K/s. The liquid $ZnCl_2$ model was overwhelmingly made up of $ZnCl_4$ tetrahedral units, with only 5% of the Zn ions being in $ZnCl_3$ or $ZnCl_5$ structural units. This small proportion could be attributed to the temperature of the melt. Although the glass was not modelled in [6], it is clear that the proportion of tetrahedral units in the glass should be 95% or higher. In addition, a Raman spectroscopy study involving liquid and glassy $ZnCl_2$ by Yannopoulos et al. [4] revealed the presence of only $ZnCl_4$ structural units, with the exception of a $ZnCl_3$ minority in the melt, which was barely detectable in the glass.

To compromise between classical and first principles molecular dynamics simulation, classical molecular dynamics simulations can be made to include ion polarizability. One approach is to use a polarizable ion model (PIM) where the dipole strength and orientation fluctuates throughout the

simulation [7]. Wilson and Madden [8] compared a liquid $ZnCl_2$ model that had been obtained using a PIM to one obtained using a RI model. It was detailed that using a RI model would maximise the Zn···Zn nearest neighbour distance, while a PIM could reproduce Zn-Cl-Zn bond bending, reducing the Zn···Zn nearest neighbour distance [8],[9]. An alternative approach for incorporating ion polarizability into classical molecular dynamics simulations is to use the core-shell model. In the core-shell model, the charge of an ion is split between a core and a shell unit which are connected by a harmonic spring of spring constant K_{cs}. The shell can either be massless (dynamic core-shell model), or have a small proportion of the atom mass (adiabatic core-shell model), and the shell movement replicates ion polarization.

Huang *et al.* [2] used the adiabatic core-shell model to produce models of $ZnCl_2$ melt. The simulation began by heating a crystalline $ZnCl_2$ structure to 2000K for 10ps prior to cooling to various temperatures (1000K, 873K, and 600K). Results consistent with experimental studies on $ZnCl_2$ melt were attained. However, the low melting temperature of 2000K coupled with a short simulation timescale may not have been sufficient in allowing a representative melt structure to develop. The results may therefore have been biased towards the input crystalline structure. Huang et al. [2] did not produce a $ZnCl_2$ glass model.

A different type of computational simulation is reverse Monte Carlo (RMC) modelling. This uses an input configuration of atoms whose positions are adjusted to reproduce experimental diffraction data. The $ZnCl_2$ glass model obtained by Pusztai and McGreevy [10] using this approach reportedly comprised of distorted tetrahedral units which had trigonal planar symmetry. The average Zn-Cl coordination number was ~3.9, and the proportions of $ZnCl_3$, $ZnCl_4$, and $ZnCl_5$ structural units were not detailed. In addition, the average Zn···Zn coordination number of ~5.3 exceeded the maximum value of 4.0 that would expected for a system comprising entirely of corner-sharing tetrahedral units.

Models of $ZnCl_2$ glass attained using RMC modelling have also been reported by Zeidler *et al.* [11], [12]. These were able to achieve average zinc and chlorine ion coordination numbers of ~4.0 and ~2.0 respectively consistent with $ZnCl_4$ structural units. However, the glass models contained significant proportions of structural units other than $ZnCl_4$ structural units. In one study, Zeidler *et al.* [12] reported that 9.8% of the structural units were either $ZnCl_3$ or $ZnCl_5$ structural units. In the later study, Zeidler *et al.* [11] reported that 41% of the chlorine ions were not two-fold coordinated and that this was "not expected." These findings could be caused by a lot of the disorder present in the initial random distribution of atoms being retained during the RMC procedure.

The present study focusses on using reliable interatomic potential parameters to model the atomic structure of $ZnCl_2$ glass without bias towards a crystalline structure, or experimental diffraction results. This was achieved using classical molecular dynamics simulation with the addition of the adiabatic core-shell model. The structure of the glass model attained was characterized using nearest neighbour distance, coordination number, bond angle distribution, ring statistics, and structure factor calculations. The influence of polarizable anions on the intermediate glass former $ZnCl_2$ were later compared to those of the strong glass former SiO_2. The SiO_2 glass system was chosen for comparison because it has been well studied both experimentally and computationally. Like $ZnCl_2$, SiO_2 shares the same AX_2 stoichiometry and comprises of AX_4 tetrahedral structural units.

Computational Methodology:

Binks [13] reports interatomic potential parameters of Buckingham form for modelling $ZnCl_2$ (table 1). The Buckingham form is expressed in equation 1, where the potential, V_{ij}, acts between ions i and j; q is the ion charge, r is the separation distance, and A, ρ, and C are potential parameters. A three-body interatomic potential of screened harmonic form (equation 2) was chosen to supplement those in table 1. This was to help ensure tetrahedral structural units through encouraging zinc ions to maintain tetrahedral coordination. In equation 2, k_3 is the spring constant, θ is the Cl-Zn-Cl bond angle, θ_0 is the equilibrium bond angle, and ρ is the potential screening distance. The adiabatic core-shell model was applied to the anions in this study. Equation 3 governs the interaction between the core and shell units, where the terms r and K_{cs} are the core-shell distance and the spring constant respectively.

Table 1: The two-body and three-body interatomic potential parameters of Buckingham and screened harmonic form respectively used to model $ZnCl_2$ glass. The subscripts 'c' and 's' correspond ion cores and ion shells respectively. The two-body interatomic potential parameters were obtained from Binks [13], whilst the three-body interatomic potential was fitted in this work.

	A (eV)	ρ (Å)	C (eV Å^6)
$Zn_c \cdots Zn_c$	0.00000	0.00000	0.00
$Zn_c - Cl_s$	9704.89	0.23200	0.00
$Cl_s \cdots Cl_s$	3296.57	0.32890	107.20
	k_3 (eV rad^{-2})	θ_0 (°)	ρ (Å)
$Cl_c - Zn_c - Cl_c$	1.5	109.47	3.0
	K_{cs} (eV Å^{-2})	Q (core) (e)	q (shell) (e)
$Cl_c - Cl_s$	17.25	0.984	-1.984
$Zn_c - Zn_c$		2.000	0.000

$$V_{ij}(r) = \frac{q_i q_j}{4\pi\epsilon_0 r} + A_{ij}\exp\left(\frac{-r}{\rho_{ij}}\right) - \frac{C_{ij}}{r^6} \quad (1)$$

$$V_{ijk}(\theta_{jik}) = \frac{k_3}{2}(\theta_{jik} - \theta_0)^2 \exp\left[-(r_{ij}^8 + r_{ik}^8)/\rho^8\right] \quad (2)$$

$$V(r) = \frac{1}{2}K_{cs}r^2 \quad (3)$$

The performance of interatomic potential parameters can be tested on crystalline structures using the General Utility Lattice Program (GULP) [14]. The δ-$ZnCl_2$ crystalline structure [15] of space group 33 is the only pure polymorph of $ZnCl_2$ as the others (α, β, and γ) occur with some water absorption [15]. Following the energy minimization of the δ-$ZnCl_2$ structure, the unit cell volume increased by 6.80% (table 2). The Zn-Cl, Cl···Cl, and Zn···Zn nearest neighbour distances of 2.27 Å, 3.77 Å, and 3.76 Å increased slightly to 2.30 Å, 3.88 Å, and 3.85 Å respectively, but the coordination numbers of 4.0, 12.0, and 4.0 respectively were maintained.

Table 2: The percentage changes to the structural parameters of the δ-$ZnCl_2$ crystalline structure following GULP energy minimisation.

Parameter	Unit	Initial value	Percent change
Volume	$Å^3$	303.59	6.80
a	Å	6.44	-1.34
b	Å	7.69	9.04
c	Å	6.13	-0.72
α	°	90.00	0.00
β	°	90.00	0.00
γ	°	90.00	0.00

A starting δ-$ZnCl_2$ crystalline configuration of 1280 atomic components (512 Cl cores, 512 corresponding Cl shells, and 256 Zn cores) of density 0.0359 $Å^{-3}$ [12] was prepared. The atomic mass of chlorine (35.453 u) was split between the anion core (35.003 u) and shell (0.450 u). A core-shell model molecular dynamics simulation was then run using DLPOLY 1.9 [16] with the interatomic potential parameters given in table 1. Initially, the simulation was run at a temperature of 6000K to ensure a random distribution of ions. The temperature was then reduced to 3000K, and then to 1000K, where the system was still comfortably above its melting temperature of 593K [17]. To form a glass model, the liquid system was quenched from 1000K to 300K at a rate of 10^{13}K/s. A further stage at 300K ensured the formation of a solid glass model. The single temperature stages and the quench stage ran for 800,000 time-steps and 350,000 time-steps respectively, where the time-step was 0.2fs. An NVT Berendsen thermostat was used throughout and all simulation stages were fully equilibrated. The SiO_2 glass model used for comparison was attained using the method reported by Tilocca et al. [18] (denoted SM1). In the following sections, the atomic correlations refer to interactions between the ion cores unless explicitly indicated otherwise (for example $Cl_s \cdots Cl_s$ refers to ion shells).

Results and Discussion:

Figure 1 illustrates a comparison between the δ-$ZnCl_2$ crystalline structure (left) and the $ZnCl_2$ glass model (right). The crystalline structure is comprised entirely of corner-sharing $ZnCl_4$ tetrahedral units, while 14% of these tetrahedral units are edge-sharing in the glass model (highlighted dark blue). This is the first fully tetrahedral model of $ZnCl_2$ glass. The magnified region of the glass at 300K shows that the chlorine shells (brown) are closer to the zinc cations than the chlorine cores (green). This is also the case in crystalline δ-$ZnCl_2$ and is a consequence of the charges assigned to the core and shell units in table 1.

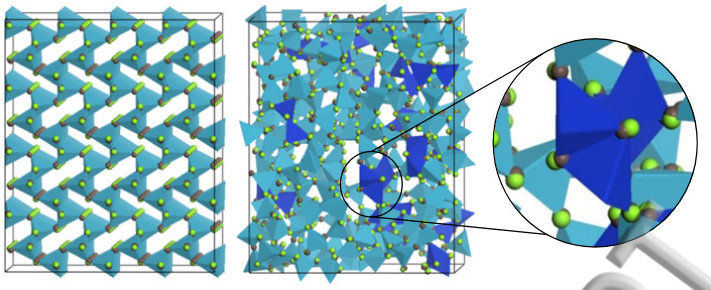

Figure 1: A model of crystalline δ-$ZnCl_2$ to the left, and a $ZnCl_2$ glass model at 300K to the right. The blue tetrahedra represent Zn ions, and the green and brown spheres correspond to Cl cores and shells respectively. In the glass model, the edge-sharing tetrahedra have been highlighted in dark blue.

The formation of these edge-sharing tetrahedra has been explained by Madden and Wilson [19] and is illustrated in figure 2. Initially, bond bending reduces the Zn···Zn separation distance, causing cation-cation repulsion to occur. A dipole in the anion is then induced. The anion-anion separation distance can then lessen to counteract the repulsion between the cations, facilitating the formation of edge-sharing tetrahedra.

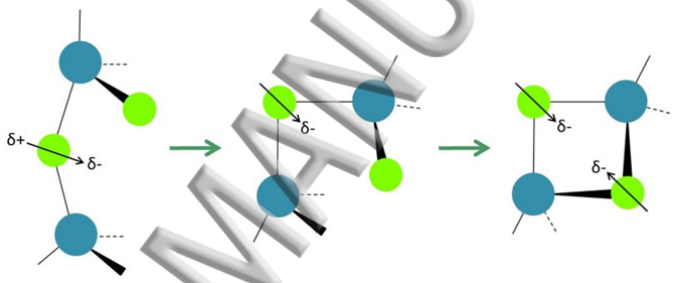

Figure 2: The formation of edge-sharing tetrahedra as discussed in Madden and Wilson [19]**. The blue and green circles represent zinc cations and chlorine anions respectively.**

The small pre-peaks visible in the Zn···Zn and Cl_s···Cl_s pair correlation functions (figure 3) are consistent with the formation of a minority of edge-sharing tetrahedra as described above. While the Zn-Cl and Cl···Cl pair correlation functions show good agreement with experimental neutron diffraction (ND) data [12] in figure 4, less good agreement is seen between the Zn···Zn pair correlation functions. The two nearest neighbour peaks in the Zn···Zn pair correlation function from this work correspond to edge-sharing and corner-sharing $ZnCl_4$ structural units. These features are also reported in the first principles study of liquid $ZnCl_2$ [6]. Conversely, only a single broad peak is observed in the experimental Zn···Zn pair correlation function [12] due to it being subject to greater uncertainty, as will be discussed in more detail below.

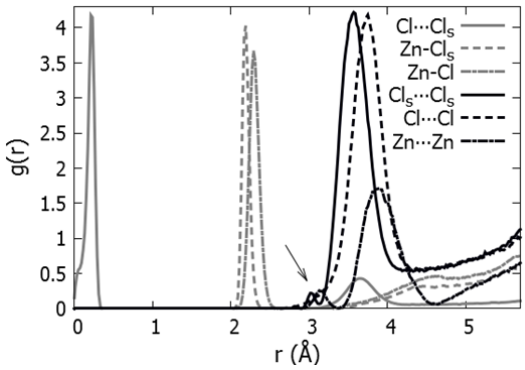

Figure 3: Pair correlation functions for $ZnCl_2$ glass. The amplitudes of the Cl···Cl$_s$, Zn-Cl$_s$ and Zn-Cl correlations were reduced by factors of 10, 4, and 3 respectively to be of similar scale to the other correlations.

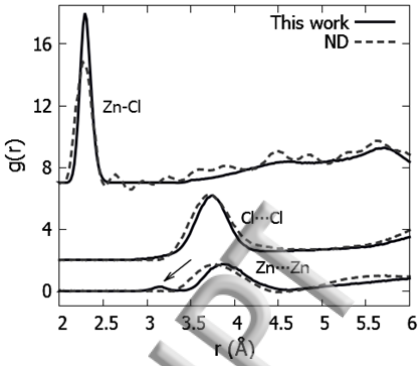

Figure 4: The Zn-Cl, Cl···Cl, and Zn···Zn pair correlation functions from this work compared with results from an ND study [12]. The Cl···Cl and Zn···Zn correlations have been offset by 2.0 and 7.0 respectively.

A summary of the nearest neighbour distances (R), coordination numbers (N(r)), and the cut-off distances applied in this work, as well as in other studies, are presented in table 3. In this work, a Zn-Cl coordination number of 4.00 is obtained. This is expected and corresponds to tetrahedral structural units. The Zn-Cl nearest neighbour distance of 2.30 Å is in line with the other studies. The Cl···Cl nearest neighbour distances are in fair agreement despite the coordination numbers varying noticeably. As shown in figure 5, the steepness of the Cl···Cl cumulative coordination number plot places a high sensitivity on the cut-off distance applied. The Zn···Zn nearest neighbour distance and coordination number values from this work are in less good agreement with those from ND experiments [12]. This is attributed to the uncertainty in the experimental Zn···Zn pair correlation function, as will be discussed in more detail below.

Table 3: Nearest neighbour distances (R), coordination numbers (N), and coordination number cut-off distances from this work and a number of other studies. These include reverse Monte Carlo (RMC), neutron diffraction (ND), x-ray diffraction (XRD), and extended x-ray absorption fine structure (EXAFS) studies. The uncertainty attributed to each value is given in parenthesis.

Ref.	Method	Zn-Cl			Cl···Cl			Zn···Zn		
		R (Å)	N(r)	Cut-off (Å)	R (Å)	N(r)	Cut-off (Å)	R (Å)	N(r)	Cut-off (Å)
This work	MD	2.30(2)	4.00(2)	3.00	3.76(5)	10.1(1)	5.00	3.89(5)	3.62(5)	4.30
[5]	MD	2.34(2)	4.96(2)	3.20	3.59(5)	11.0(1)	4.50	3.81(5)	5.3(1)	4.50
[10]	RMC	2.34(2)	3.91(2)	3.00	3.71(5)	10.8(1)	4.70	3.79(5)	5.28(5)	4.70
[12]	RMC	2.29(5)	3.99(1)	3.00	3.69(5)	12.2(1)	5.00	3.67(5)	4.16(1)	4.30
[12]	XRD	2.27(2)	4.0(1)	2.47						
[12]	ND	2.27(1)	3.8(3)	2.52	3.68(1)	11.0(4)	4.66	3.74(1)	3.8(2)	4.42
[11]	ND	2.27(2)	4.04(5)							
[20]	ND	2.29(1)	3.8		3.72(1)	9.5				
[21]	EXAFS	2.30(4)								

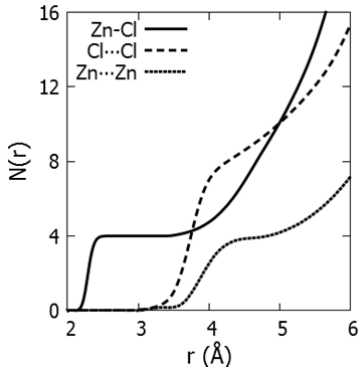

Figure 5: Cumulative coordination number plots for the Zn-Cl, Cl···Cl and Zn···Zn correlations of $ZnCl_2$ glass.

Figure 6 depicts the bond angle distributions (BADs) in the $ZnCl_2$ glass model. The average angle in the Cl-Zn-Cl bond angle distribution is 109°, matching the ideal tetrahedral angle [12]. The Zn-Cl-Zn BAD in figure 6 shows two clear peaks. The same observation was made in the first principles study of liquid $ZnCl_2$ [6]. The first peak corresponds to edge-sharing tetrahedra while the second peak corresponds to corner-sharing tetrahedra. The amplitude of the corner-sharing peak is greater due to the dominant number of corner-sharing units. Whilst 14% of the tetrahedra are edge-sharing, 86% are corner-sharing. In contrast, RMC simulations [10]–[12] produce more disordered Zn-Cl-Zn BADs with only a single broad peak.

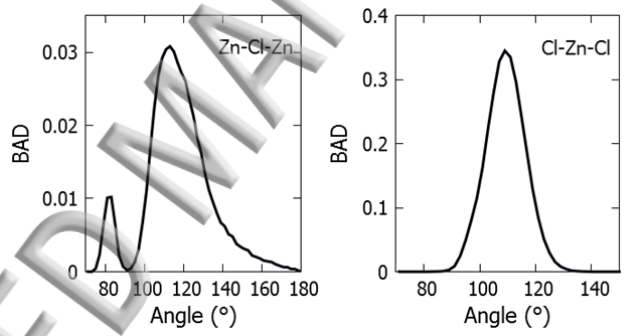

Figure 6: The Zn-Cl-Zn bond angle distribution to the left, and the Cl-Zn-Cl distribution to the right for $ZnCl_2$ glass.

As the $ZnCl_2$ glass model comprises of a fully tetrahedral and highly corner-sharing network, it is also of interest to investigate the ring statistics. Figure 7 presents the ring size distribution in terms of the number of tetrahedra in a ring, n. In figure 7, the first measure, $R_C(n)$, represents the shortest n-membered ring for each of the six X-A-X segments in a AX_4 tetrahedra. The second measure, $P_N(n)$, represents the proportion of tetrahedra for which the shortest ring is an n-membered ring. Hence, $P_N(n)$ is weighted to smaller ring sizes compared to $R_C(n)$. It can be seen in figure 7 that both $R_C(n)$ and $P_N(n)$ show some 2-membered rings which correspond to the edge-sharing of $ZnCl_4$ tetrahedra. In addition, there is a noticeable excess of 3-membered rings which are possibly due the Zn-Cl-Zn inter-tetrahedral bond angles centred around 110°. Lastly, the bulk of the ring size distributions are concentrated around 6 to 8-membered rings.

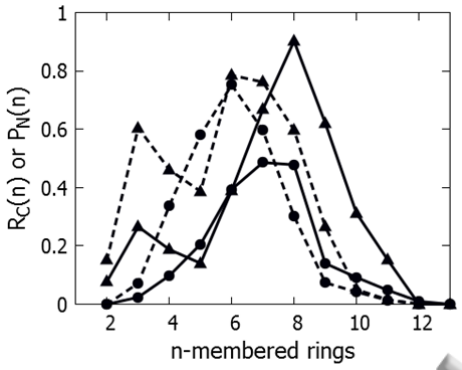

Figure 7: The distributions of rings containing n AX_4 tetrahedra in models of $ZnCl_2$ (triangles) and SiO_2 (circles) glass. The two measures shown are $R_c(n)$ (solid lines) which is the shortest ring per X-A-X segment of a AX_4 tetrahedra, and $P_n(n)$ (dashed lines) which is the proportion of AX_4 tetrahedra for which the shortest ring is an n-membered ring.

Figure 7 also includes the ring statistics for the model of the strong glass former SiO_2. This enables comparisons to be made with the model of the intermediate glass former $ZnCl_2$. The ring statistics for SiO_2 are consistent with those previously reported [22], [23] and show that the bulk of the ring size distribution is concentrated around 6 to 7-membered rings. These are somewhat smaller than in $ZnCl_2$ glass. This may be due to a tendency for larger values of n to occur in $ZnCl_2$ glass when edge-sharing tetrahedra are present in the ring. Other differences between the ring statistics of $ZnCl_2$ and SiO_2 are that the latter has no 2-membered rings, and very few 3-membered rings which are regarded as defects due to the average Si-O-Si bond angle of ~150° [24].

The total neutron and x-ray structure factors, $S(Q)$, for the $ZnCl_2$ glass model were calculated according to equation 4. The Faber-Ziman (FZ) partial structure factors, $S_{ij}^{FZ}(Q)$, were calculated according to equations 5 (which is equivalent to equation 6 in [25]). In equations 4 and 5, the term Q is the scattering vector, i and j are atom types, c is the fractional concentration, $g(r)$ is the pair correlation function, r is a radial distance, and ρ is the atomic number density. The weighting factors are $\omega_{ij} = \frac{(2-\delta_{ij})c_i c_j b_i b_j}{[\bar{b}]^2}$ for neutrons and $\omega_{ij} = \frac{(2-\delta_{ij})c_i c_j z_i z_j}{[\bar{z}]^2}$ for x-rays, where the terms δ, b, and z correspond to a Kronecker delta function, the neutron scattering length, and the atomic number respectively.

$$S(Q) = 1 + \int_0^\infty \sum_{ij} \frac{\omega_{ij}}{c_j}\left(g_{ij}(r) - 4\pi r\rho_j\right)\frac{\sin(Qr)}{Q}\,dr \qquad (4)$$

$$S_{ij}^{FZ}(Q) = 1 + \int_0^\infty \frac{1}{c_j}\left(g_{ij}(r) - 4\pi r\rho_j\right)\frac{\sin(Qr)}{Q}\,dr \qquad (5)$$

The modelled total neutron and x-ray structure factors shown in figure 8 closely resemble those from neutron and x-ray diffraction experiments [11], [12]. In addition, the modelled FZ partial structure factors shown in figure 9 agree particularly well with experimental ND results [12]. However, there is some discrepancy between the experimental and simulated $S_{ZnZn}^{FZ}(Q)$ plots. The noise in $S_{ZnZn}^{FZ}(Q)$ from ND [12] was caused by the Zn···Zn partial structure factor having a lower signal-to-noise ratio due to its weak weighting of $\omega_{ZnZn} = 0.05$ in comparison to the total structure factor where $\omega_{ZnCl} = 0.35$ and $\omega_{ClCl} = 0.59$. This noise caused the experimental Zn···Zn pair correlation function to be of poor resolution, explaining why small features like the pre-peak

This manuscript was accepted by J. Chem. Phys. Click here to see the version of record.

indicated by arrows in figures 3 and 4 cannot be resolved. Soper [26] discusses the challenging nature of attaining Zn···Zn pair correlation functions experimentally, stating that a range of Zn···Zn pair correlation functions can represent experimental data equally well.

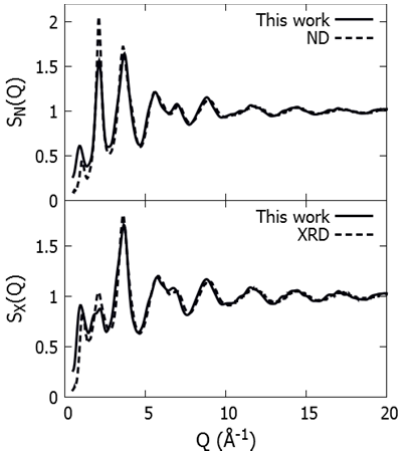

Figure 8: Computed total neutron and x-ray structure factors for $ZnCl_2$ glass compared with experimental neutron [12] and x-ray diffraction data [11].

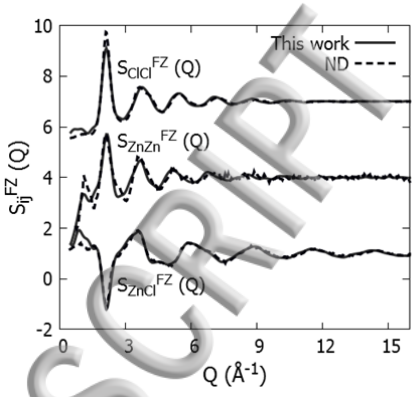

Figure 9: Calculated Faber-Ziman partial structure factors compared with neutron diffraction data [12]. The $S_{ZnZn}^{FZ}(Q)$ and $S_{ClCl}^{FZ}(Q)$ plots have a vertical offset of 3.0 and 6.0 respectively.

To make further comparisons between the $ZnCl_2$ and SiO_2 glass models, table 4 compares the positions of the first three peaks in the total correlation functions (R_1, R_2, and R_3), and the first three peaks in the total neutron structure factors (Q_1, Q_2, and Q_3). Through comparing the Si-O and Zn-Cl bond lengths, R_1, it can be found that a SiO_4 tetrahedral unit is 1.42 times smaller than a $ZnCl_4$ tetrahedral unit. As expected, a similar ratio is found for the anion-anion nearest neighbour distance (R_2), which corresponds to the edge length of a tetrahedral unit. This would appear to explain the observed ratios of ~1.4 for the second and third diffraction peak positions (Q_2 and Q_3). The cation-cation nearest neighbour distance (R_3) ratio is smaller with a value of 1.25. This is because the average Zn-Cl-Zn bond angle of ~110° is smaller than the average Si-O-Si bond angle of ~150° [24]. This reduces the Zn···Zn nearest neighbour distance, and hence lowers the R_3 ratio compared to the R_1 and R_2 ratios.

Table 4: The cation-anion (R_1), anion-anion (R_2), and cation-cation (R_3) nearest neighbour distances, as well as the first three peak positions (Q_1, Q_2 and Q_3) in the total neutron structure factors. The uncertainty in the R and Q values is ±0.01 Å and ±0.05 Å^{-1} respectively.

	R_1 (Å)	R_2 (Å)	R_3 (Å)	Q_1 (Å^{-1})	Q_2 (Å^{-1})	Q_3 (Å^{-1})
$ZnCl_2$	2.30	3.76	3.89	0.88	2.11	3.69
SiO_2	1.62	2.64	3.11	1.53	2.91	5.19
Ratio	1.42	1.42	1.25	1.74	1.38	1.41

In order to compare the FZ partial structure factors of the $ZnCl_2$ and SiO_2 glass models, it is necessary to account for the different Q ratios. This can be achieved by scaling the Q values using the relation $Q'=Q\times R_{ij}$, where R_{ij} is the i-j nearest neighbour distance. Figure 10 shows that the scaled FZ partial structure factors have strong similarities beyond the first sharp diffraction peak (FSDP). This is due

This manuscript was accepted by J. Chem. Phys. Click here to see the version of record.

to both of the networks comprising of dominantly corner-sharing tetrahedral structural units. The FSDPs however need to be explored further.

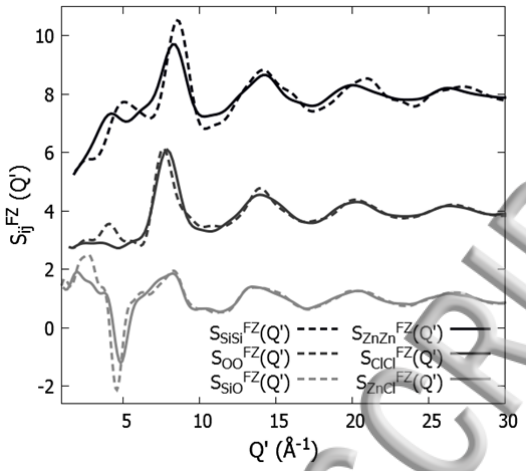

Figure 10: A Faber-Ziman partial structure factor comparison between $ZnCl_2$ and SiO_2 using a normalized Q scale of Q'=Q×R_{ij}, where R_{ij} is the i-j nearest neighbour distance. The vertical offset for the $S_{\mathrm{ZnZn}}^{FZ}(Q')$ and $S_{\mathrm{SiSi}}^{FZ}(Q')$ plots is 7.0. The $S_{\mathrm{ClCl}}^{FZ}(Q')$ and $S_{\mathrm{OO}}^{FZ}(Q')$ plots have an offset of 3.0.

The FSDPs of $ZnCl_2$ and SiO_2 are seen at Q_1 values of 0.88 Å^{-1} and 1.53 Å^{-1} respectively (table 4). As it is unclear why the Q_1 ratio of 1.74 is noticeably greater than the other ratios, it is of interest to view the FSDPs more in more detail (figure 11). Madden and Wilson reported that the FSDP in MD models of liquid $ZnCl_2$ were almost exclusively caused by $S_{\mathrm{ZnZn}}^{FZ}(Q)$ [8]. However, this cannot be the case due to its weak weighting as discussed above. In $ZnCl_2$, the weighting factors are $\omega_{ZnCl} = 0.35$, $\omega_{ClCl} = 0.59$, and $\omega_{ZnZn} = 0.05$. In SiO_2, the weighting factors are $\omega_{SiO} = 0.39$, $\omega_{OO} = 0.54$, and $\omega_{SiSi} = 0.07$. Instead, Soper [26] and Neuefeind [27] considered that the FSDP was mainly caused by $S_{\mathrm{ZnCl}}^{FZ}(Q)$. This latter viewpoint is supported by the total and partial neutron structure factors for the MD model of $ZnCl_2$ glass in figure 11. It can also be noticed that this parallels with the case of SiO_2, where the most significant contribution to the FSDP also comes from the cation-anion contribution, i.e. $S_{\mathrm{SiO}}^{FZ}(Q)$. It still remains unclear why the Q_1 ratio for the FSDP is higher than that of the Q_2 and Q_3 ratios.

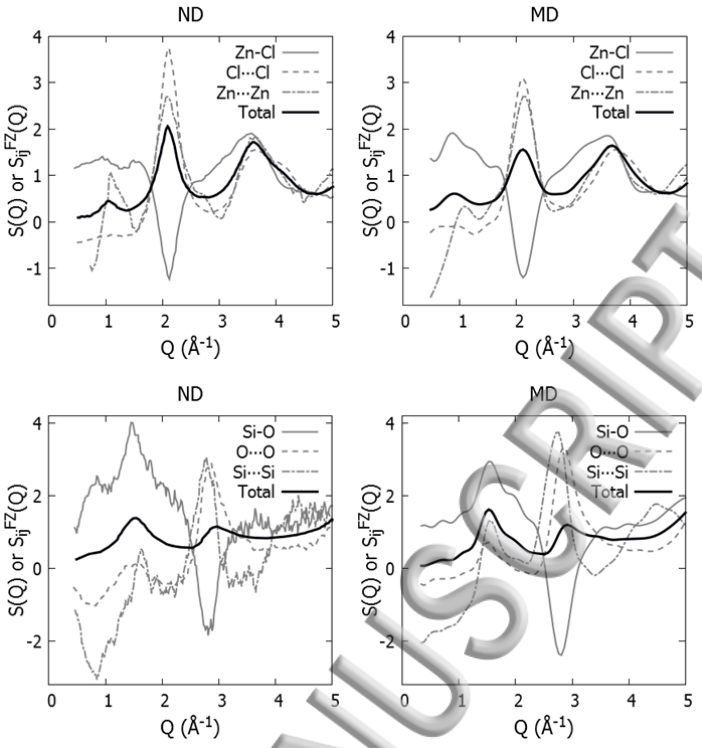

Figure 11 Total neutron structure factors and Faber-Ziman partial structure factors for $ZnCl_2$ and SiO_2. The plots to the left were obtained from neutron diffraction (ND) experiments [12], [28], [29] **and the plots to the right were from molecular dynamics simulation (MD) in this study.**

Conclusion:

The intermediate glass former $ZnCl_2$ was modelled computationally using classical molecular dynamics. The effects of anion polarizability were incorporated using the adiabatic core-shell model. The $ZnCl_2$ glass model attained was fully tetrahedral, and 14% of the tetrahedral units were found to be edge-sharing. The $ZnCl_2$ glass model was able to closely reproduce experimental neutron and x-ray structure factors. The model provides clear details in the Zn···Zn pair correlation function which are unobtainable from diffraction experiments due to the weak weighting of the correlation. Models of the intermediate glass former $ZnCl_2$ and the strong glass former SiO_2 were also compared in this work. The ring size distributions in the $ZnCl_2$ glass model showed a significant number of 3-membered rings, whilst these were only present as defects in the SiO_2 glass model. There were strong similarities between the FZ partial structure factors of $ZnCl_2$ and SiO_2 glass once they were scaled according to nearest neighbour distances. This was understandable because both have a dominantly corner-sharing tetrahedral network. By analyzing the FZ partial structure factors of the $ZnCl_2$ and SiO_2 glass models further, it was found that the main contribution to the FSDP came from the cation-anion contribution in both cases. Interestingly, the FSDP positions in the $ZnCl_2$ and SiO_2 glass models do not follow a scaling relation that is based on nearest neighbour distances.

Acknowledgements:

The authors are grateful to the EPSRC for funding.

References:

[1] B. K. Sharma and M. Wilson, "Polyamorphism and the evolution of intermediate-range order in molten $ZnCl_2$," *J. Phys. Condens. Matter*, vol. 20, pp. 244123–244132, 2008.

[2] S. Huang, F. Yoshida, and W. Wang, "The structural and dynamical properties of $ZnCl_2$ melt—a molecular dynamics simulation study," *J. Mol. Liq.*, vol. 115, pp. 81–88, 2004.

[3] I. T. Penfold and P. S. Salmon, "Structure of covalently bonded glass-forming melts: A full partial-structure-factor analysis of liquid $GeSe_2$," *Phys. Rev. Lett.*, vol. 68, no. 1, p. 252, 1992.

[4] S. N. Yannopoulos, A. G. Kalampounias, A. Chrissanthopoulos, and G. N. Papatheodorou, "Temperature induced changes on the structure and the dynamics of the 'tetrahedral' glasses and melts of $ZnCl_2$ and $ZnBr_2$," *J. Chem. Phys.*, vol. 118, no. 7, pp. 3197–3214, 2003.

[5] P. N. Kumta, P. A. Deymier, and S. H. Risbud, "Glass formation in simple ionic systems via constant pressure molecular dynamics," *J. Chem. Phys.*, vol. 90, no. 12, p. 7384, 1989.

[6] A. Q. Alsayoud, M. Venkateswara Rao, A. N. Edwards, P. A. Deymier, K. Muralidharan, B. G. Potter, K. Runge, and P. Lucas, "Structure of $ZnCl_2$ melt. Part I: Raman spectroscopy analysis driven by Ab initio methods," *J. Phys. Chem. B*, vol. 120, no. 17, pp. 4174–4181, 2016.

[7] M. Wilson and P. A. Madden, "Polarization effects in ionic systems from first principles," *J. Phys. Condens. Matter*, vol. 5, no. 17, pp. 2687–2706, 1999.

[8] M. Wilson and P. Madden, "Voids, Layers, and the First Sharp Diffraction Peak in $ZnCl_2$," *Phys. Rev. Lett.*, vol. 80, no. 3, pp. 532–535, 1998.

[9] M. Wilson and P. A. Madden, "Short- and intermediate-range order in MCl_2 melts: the importance of anionic polarization," *J. Phys. Condens. Matter*, vol. 5, no. 37, pp. 6833–6844, 1993.

[10] L. Pusztai and R. L. McGreevy, "The Structure of Glassy Zinc Chloride: A Reverse Monte Carlo

Study," *J. Non. Cryst. Solids*, vol. 117/118, pp. 627–630, 1990.

[11] A. Zeidler, P. Chirawatkul, P. S. Salmon, T. Usuki, S. Kohara, H. E. Fischer, and W. S. Howells, "Structure of the network glass-former $ZnCl_2$: From the boiling point to the glass," *J. Non. Cryst. Solids*, vol. 407, pp. 235–245, 2015.

[12] A. Zeidler, P. S. Salmon, R. A. Martin, T. Usuki, P. E. Mason, G. J. Cuello, S. Kohara, and H. E. Fischer, "Structure of liquid and glassy $ZnCl_2$," *Phys. Rev. B - Condens. Matter Mater. Phys.*, vol. 82, pp. 1–17, 2010.

[13] D. J. Binks, "Computational Modelling of Zinc Oxide and Related Oxide Ceramics," 1994.

[14] J. D. Gale and A. L. Rohl, "The General Utility Lattice Program (GULP)," *Mol. Simul.*, vol. 29, no. 5, pp. 291–341, 2003.

[15] J. Yakel, H. L., Brynestad, "Refinement of the crystal structure of orthorhombic zinc chloride," *Inorg. Chem.*, vol. 17, no. 11, pp. 3294–3296, 1978.

[16] W. Smith and T. R. Forester, "DL_POLY_2. 0: A general-purpose parallel molecular dynamics simulation package," *J. Mol. Graph.*, vol. 14, no. 3, pp. 136–141, 1996.

[17] A. Sen, M. N. Rao, R. Mittal, and S. L. Chaplot, "Collective dynamics in crystalline polymorphs of $ZnCl_2$: potential modelling and inelastic neutron scattering study," *J. Phys. Condens. Matter*, vol. 17, pp. 6179–6192, 2005.

[18] A. Tilocca, N. H. De Leeuw, and A. N. Cormack, "Shell-model molecular dynamics calculations of modified silicate glasses," *Phys. Rev. B - Condens. Matter Mater. Phys.*, vol. 73, pp. 1–14, 2006.

[19] P. A. Madden and M. Wilson, "'Covalent' effects in 'ionic' liquids," *J. Phys. Condens. Matter*, vol. 12, pp. 95–108, 2000.

[20] J. A. E. Desa, A. C. Wright, J. Wong, and R. N. Sinclair, "A neutron-diffraction investigation of the structure of vitreous zinc-chloride," *J. Non. Cryst. Solids*, vol. 51, pp. 57–86, 1982.

[21] C. Fillaux, B. Couzinet, C. Dreyfus, J. P. Itié, and A. Polian, "Determination of the Short Range Structure of $ZnCl_2$ in its Liquid, Vitreous and Crystalline Phases by XAS, at High Pressure and

High Temperature," *Phys. Scr.*, vol. 115, pp. 339–341, 2005.

[22] R. M. Van Ginhoven, H. Jónsson, and L. R. Corrales, "Silica glass structure generation for *ab initio* calculations using small samples of amorphous silica," *Phys. Rev. B*, vol. 71, no. 2, p. 24208, 2005.

[23] X. Yuan and A. N. Cormack, "Efficient algorithm for primitive ring statistics in topological networks," *Comput. Mater. Sci.*, vol. 24, no. 3, pp. 343–360, 2002.

[24] D. L. Price, M. L. Saboungi, S. Susman, K. J. Volin, and A. C. Wright, "Dynamics of vitreous and molten zinc chloride," *J., Non-Cryst. Solids*, vol. 150, pp. 287–291, 1992.

[25] D. A. Keen, "A comparison of various commonly used correlation functions for describing total scattering," *J. Appl. Cryst.*, vol. 34, pp. 172–177, 2001.

[26] A. K. Soper, "The structure of molten $ZnCl_2$: A new analysis of some old data," *Pramana - J. Phys.*, vol. 63, no. 1, pp. 41–50, 2004.

[27] J. Neuefeind, K. Tödheide, A. Lemke, and H. Bertagnolli, "The structure of molten $ZnCl_2$," *J. Non. Cryst. Solids*, vol. 224, no. 3, pp. 205–215, 1998.

[28] Q. Mei, C. J. Benmore, S. Sen, R. Sharma, and J. L. Yarger, "Intermediate range order in vitreous silica from a partial structure factor analysis," *Phys. Rev. B - Condens. Matter Mater. Phys.*, vol. 78, no. 14, pp. 144204–144211, 2008.

[29] D. I. Grimley, A. C. Wright, and R. N. Sinclair, "Neutron scattering from vitreous silica IV. Time-of-flight diffraction," *J. Non. Cryst. Solids*, vol. 119, no. 1, pp. 49–64, 1990.